J Electr Eng Technol.2017; 12(4): 1484-1494
http://doi.org/10.5370/JEET.2017.12.4.1484

ISSN(Print) 1975-0102
ISSN(Online) 2093-7423

An Efficient and High-gain Inverter Based on The 3S Inverter Employs Model Predictive Control for PV Applications

Omar Abdel-Rahim†, Hirohito Funato* and Haruna Junnosuke*

Abstract – We present a two-stage inverter with high step-up conversion ratio engaging modified finite-set Model Predictive Control (MPC) for utility-integrated photovoltaic (PV) applications. The anticipated arrangement is fit for low power PV uses, the calculated efficiency at 150 W input power and 19 times boosting ratio was around 94%. The suggested high-gain dc-dc converter based on Cockcroft-Walton multiplier constitutes the first-stage of the offered structure, due to its high step-up ability. It can boost the input voltage up to 20 times. The 3S current-source inverter constitutes the second-stage. The 3S current-source inverter hires three semiconductor switches, in which one is functioning at high-frequency and the others are operating at fundamental-frequency. The high-switching pulses are varied in the procedure of unidirectional sine-wave to engender a current coordinated with the utility-voltage. The unidirectional current is shaped into alternating current by the synchronized push-pull configuration. The MPC process are intended to control the scheme and achieve the subsequent tasks, take out the Maximum Power (MP) from the PV, step-up the PV voltage, and introduces low current with low Total Harmonic Distortion (THD) and with unity power factor with the grid voltage.

Keywords: High-gain dc-dc converter, Cockcroft-Walton multiplier, Model predictive control, 3S current source inverter, Utility-integrated, Total Harmonic Distortion (THD)

1. Introduction

PV micro-inverters are required to step-up the PV voltage, and convert dc voltage into ac voltage and inject a sinusoidal current in phase with the grid voltage, in case of grid integration. Some PV micro-inverters topologies use a two stages in order to achieve the requirement [1-7]. Grid-connected inverters can be assorted as one stage or double stages inverters according to the number of stages used between the PV and the grid [10-15]. Double stages topology consists of a dc / dc converter that magnifies the PV module voltage to a sufficient voltage-level and performs maximum power point tracking (MPPT). The inversion stage controls the grid current to be sinusoidal and in phase with the grid voltage [8, 9]. The dc capacitor performs power decoupling. Reducing the number of power stages helps increasing the overall efficiency and the reliability of the grid-connected inverter as well as reduces the cost of increasing power density [16]. Single-stage inverter can perform all the desired functionalities developed by the two-stage topologies [17-19].

MPC related to a wide family of controllers. The principle of operation of this type of controller are that it uses a model of the system to predict the future behavior of the variables until a predefined horizon in time, and selection of the optimal actuations by minimizing a cost function. This structure has several important advantages [20-22]:

- Concepts are very intuitive and easy to understand.
- It can be applied to a great variety of systems.
- Easy inclusion of non-linearity in the model.
- Simple treatment of constraints.

However, some disadvantages have to be mentioned, like:

- The larger number of calculations, compared to classic controllers.
- And if the parameters of the system change in time, some adaptation or estimation algorithm has to be considered.

The advised structure is portrayed in Fig. 1. It assembled from PV module, the high gain dc-dc converter, the 3S current-source inverter, and utility-grid. The high-gain converter steps-up PV voltage to an adequate voltage level suitable for grid integration and to take out the maximum available power from the PV module. The 3S current source inverter inserts a current that is sinusoidal and has unity power factor reading to the grid voltage. MPC represents the control circuit. The MPC algorithm takes out the PV module MP and controls the grid current to be sinusoidal and in phase with the grid voltage.

† Corresponding Author: Dept. of Electrical and Electronic Engineering, Faculty of Engineering, Aswan University, Egypt. (o.abdelrahim@aswu.edu.eg)
* Dept. of Electrical and Electronic Engineering, Utsunomiya University, Japan. (funato@cc.utsunomiya-u.ac.jp, haruna1171@gmail.com)
Received: November 9, 2016; Accepted: June 22, 2017

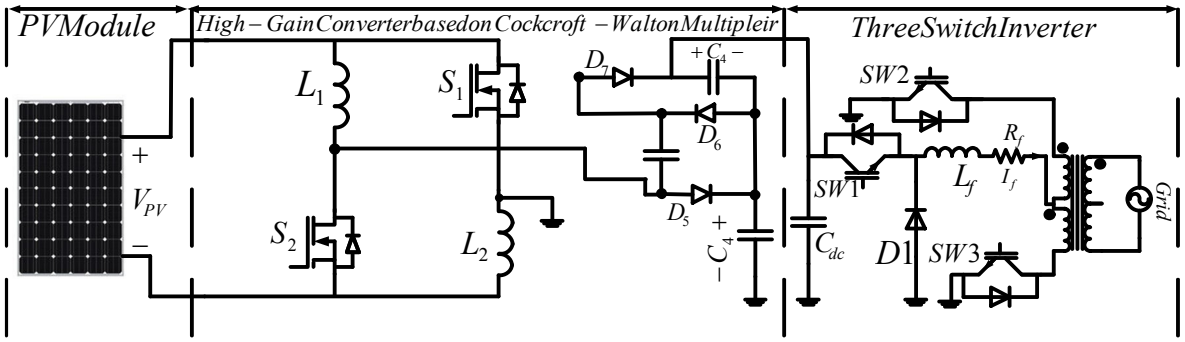

Fig. 1. Structure of the proposed system

This paper contributes the following:

- Suggestion of a MPC algorithm for the proposed system to do the upcoming tasks:
  - pull out the MP from the PV module
  - adjust the boosting ratio of the high gain dc-dc converter
  - control the active and reactive power injected into the grid
  - Optimize the switching states to reduce the switching losses of the system.
- Utilization of the 3-S current source inverter in PV applications owing to its inherent features over the traditional H-bridge inverter, such as galvanic isolation, reduced switching losses, less number of power devices and higher efficiency.
- Offering high gain dc-dc converter that can provides high gain with high efficiency based on the Cockcroft-Walton voltage amplifier.

2. Proposed High Gain DC-DC Converter Based on Cockcroft-Walton Multiplier

A transformer less dc–dc high step-up converter is proposed in this section, as shown in Fig. 2. Compared with the switched inductor boost converter [23], the proposed converter has the following merits:

1) Two power devices exist in the current-flow path during the switch-on period, and one power device exists in the current-flow path during the switch-off period;
2) The voltage stresses on the active switches are less than half of the output voltage; and
3) Under the same operating conditions, including input voltage, output voltage, and output power, the current stresses on the active switch during the switch-on period is equal to the half of the current stress on the active switch of the converter in [24].

Fig. 2(a) displays the circuit configuration of the suggested converter, which consists of two active switches, two inductors that have the same level of inductance, three diodes, and three capacitors. Switches S1 and S2 are

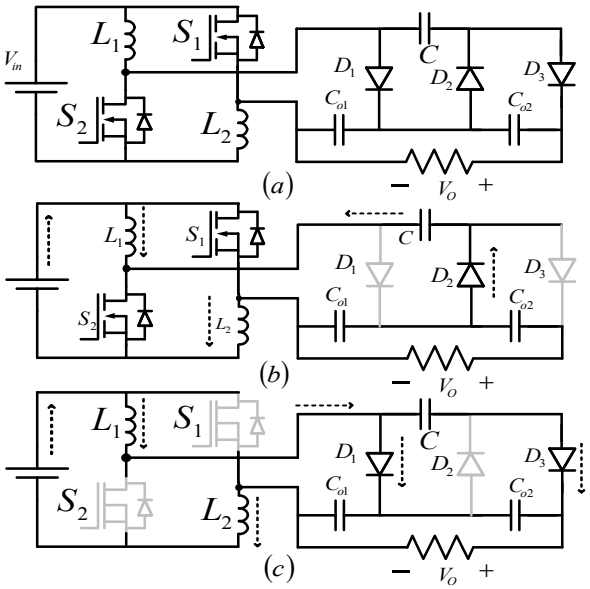

Fig. 2. Proposed converter and its modes of operation (a) proposed topology (b) mode1 (c) mode2

controlled simultaneously by using one control signal. Fig. 3 illustrates some typical waveforms obtained during continuous conduction mode (CCM). The operating principles and steady-state analysis of CCM are presented in detail as follows.

Mode 1 takes place when switches $S1$ and $S2$ are triggered to be on, as revealed in Fig. 2(b). Turning-on switches $S1$ and $S2$ lead diode $D2$ to have forward voltage so it becomes on. While diodes $D1$ and $D3$ have reverse voltages and they turned off. The main descriptive equations of this mode are as follow:

$$\mathrm{v_{L1}(t) = v_{L2}(t) = V}_{in} \tag{1}$$

$$i_{in} = 2i_L \tag{2}$$

$$v_o = v_{co1} + v_{co2} \tag{3}$$

$$v_c = v_{co1} + v_{in} \tag{4}$$

Mode 2 takes place when switches $S1$ and $S2$ are triggered to be off, as shown in Fig. 2(c). Turning off the switches $S1$ and $S2$. Diode $D2$ will have reverse voltage

and will turned off. While diodes $D1$, and $D2$ will have forward voltages and they become on. The main descriptive equations of this mode are as follow:

$$v_{L1}(t) = v_{L2}(t) = (V_{in} - \frac{V_o}{2})/2 \quad (5)$$

$$i_{in} = i_L \quad (6)$$

$$v_o = v_{co1} + v_{co2} \quad (7)$$

$$v_c = v_{co2} \quad (8)$$

Applying inductor voltage second balance and capacitor charge balance, the voltage gain of the proposed converter could be obtained as follow:

$$V_{in}.D + \frac{V_{in}}{2}.(1 - \mathrm{D}) - \frac{V_{co1}}{2}.(1 - D) = 0 \quad (9)$$

From Eqs. (3), (4), (7) and (8), capacitor $co1$ voltage can be obtained, and it is defined as

$$V_{co1} = {}^{V_o}/_2 - {}^{V_{in}}/_2 \quad (10)$$

$$V_{co2} = V_c = {}^{V_o}/_2 + {}^{V_{in}}/_2 \quad (11)$$

Substitute Eq. (10) into Eq. (9), the voltage gain of the proposed converter can be obtained. The voltage gain of the proposed converter is indicated by Eq. (12) and relation between input current and inductor current is shown in Eq. (13) and it is derived from Eqs. (2) and (6).

$$\frac{V_o}{V_g} = M = \frac{(3+\mathrm{D})}{(1-D)} \quad (12)$$

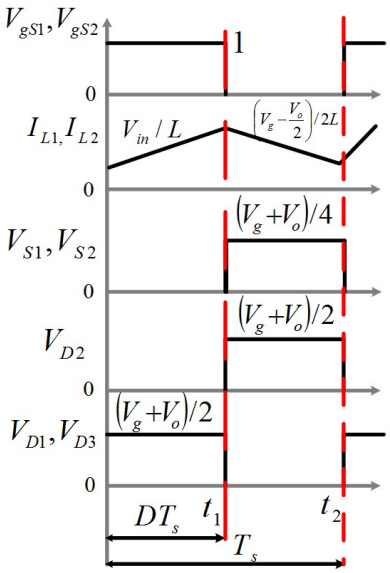

Fig. 3. Converter typical waveforms

Table 1. Proposed converter components voltage stress.

Comp.	Voltage stress	Comp.	Voltage Stress
S1=S2	Vo/4+Vin/4	D3	Vo/2+Vin/2
D1	Vo/2+Vin/2	D2	Vo/2+Vin/2

$$I_{in} = (1 + D)I_{L1} \quad (13)$$

The proposed high gain converter has two switches, three diodes, two inductors and two output capacitor. The voltage stresses of each device is depicted in 0, as can be seen from the table, the two switches have reduced voltage stresses and they are equal to quarter of the summation of input and output voltage. The three diodes have the same voltage stress around half of the sum of the input and output voltage.

Fig. 4 represent the relation between efficiency and input power at different voltage gain. These results are calculated with the help of PSIM software. Circuit parameters used in efficiency calculation are depicted in 0. Input power is studied up to 200 W. The system is studied at different voltage gains, results are depicted in Fig. 4. As can be deducted from the graph, the proposed converter can give voltage gain up to 18 times. Efficiency affected by the voltage gain and amount of input power. The converter has higher efficiency at lower power, and it reduces with increase in power. is not suitable for application required low voltage gain, as it can be seen that at voltage gain equal to 8 and input power between 100 to 150 W the efficiency is around 91%. With increase in the boosting ratio, with the same power level, the efficiency of the proposed high gain converter becomes better for example at voltage gain G=18 the efficiency of the proposed converter is 95%.

2.1 Discretization

The Euler forward method is used to get a discrete-time model, using

$$\frac{di_L(t)}{dt} = \frac{I_L(k+1) - I_L(k)}{T_s}. \quad (14)$$

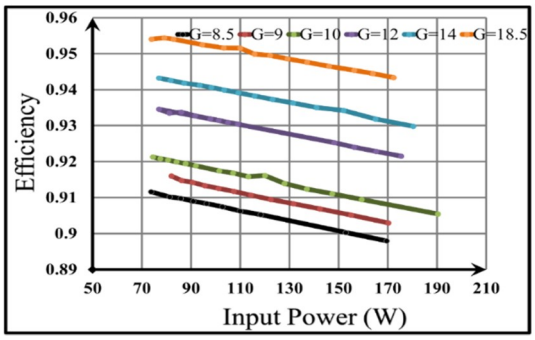

Fig. 4. Calculated efficiency of the proposed converter versus the input power and voltage gain

Table 1. Circuit parameter used to simulate the proposed converter

Component	Value	Component	Value
RL1=RL2	10 mΩ	D1=D2=D3	0.5 V
Ron	0.2 Ω	Fs	30 KHz

where T_s is the sampling time. The discretisation of the converter equations can be derived as follow:

When the switch SW is on.

$$I_{PV,1} = I_{L1}(k+1) = I_{L2}(k+1) = \frac{T_S}{L1}.\left(V_{pv}(k)\right) + I_{L1}(K).\left(1-(R_{on}+R_{L1})\right) \quad (15)$$

When switch SW is off, the discrete equation is expressed as follows:

$$I_{L1}(k+1) = I_{L2}(k+1) = \frac{T_S}{2L1}\left(V_{pv}(k) - {}^{V_o}/_{2}\right) + I_{L1}(K)\left(1-\frac{T_S}{L1}R_{L1}\right) \quad (16)$$

And hence

$$I_{PV,0} = \frac{T_S}{L1}\left(V_{pv}(k) - {}^{V_o}/_{2}\right) + I_{L1}(K)\left(1-\frac{2T_S}{L1}R_{L1}\right) \quad (17)$$

Eq. (15) and (17) represent the possible predicted values of the controlled PV current.

Last stage for the MPC algorithm is the optimization stage, where the cost function with the least error is selected. The key parameter of the MPC is the cost function because it determines the required control functions. Two cost function are compared at the optimization stage, the cost function when the switch is turned off, which is indicated as $G_{i,0}$, and the cost function when the switch is turned on, which is indicated as $G_{i,1}$.

$$G_{i,0} = \left|I_{pv,0}(k+1) - I_{ref,PV}\right| \quad (18)$$

$$G_{i,1} = \left|I_{pv,1}(k+1) - I_{ref,PV}\right| \quad (19)$$

where $I_{pv,0}(k+1)$, $I_{pv,1}(k+1)$, I_{ref}, R_{on} and R_{L1} represent the PV module upcoming current when the switch is turned off, PV module upcoming current when the switch is turned on, Incremental Conduction (IC) algorithm generated reference current, switch on resistance, and L1 series resistance, respectively.

3. Model Predictive Control for the 3S Inverter

The 3-switch current source inverter, depicted in Fig. 5, has 2 zero vectors and 2 positive active vectors. During positive half cycle only positive vector is used, while in negative half cycle only negative vector is used.

(1) It is capable of generating an AC output voltage of any desired frequency (50 Hz / 60 Hz) by employing three power semiconductor switches, in which only one is operating at high frequency and other two are operating at fundamental frequency,
(2) It produces a sine wave output voltage without using any filter at its output,
(3) It possesses only three power semiconductor switches and results in minimized control complexity, low switching loss, high efficiency, enhanced performance and less cost,
(4) It possesses galvanic isolation between input DC and output AC because of the fundamental frequency transformer

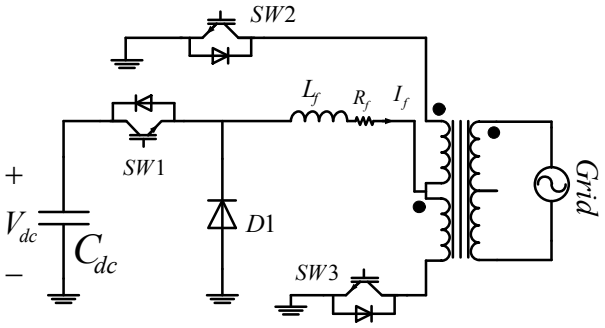

Fig. 5. Grid connected three-switch inverter

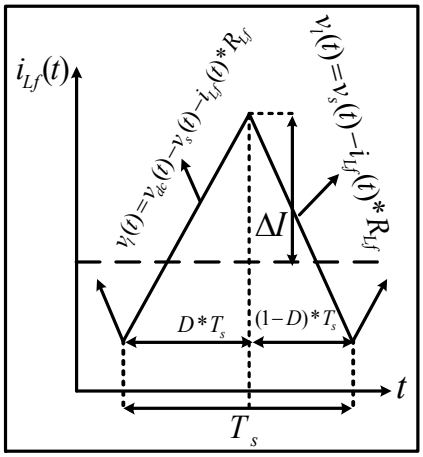

Fig. 6. Filter inductor current

All possible switching states are depicted in Fig. 6. Positive half cycle has two possible states, and negative half cycle has two states as follows:

1. Switches sw1, and sw3 are turned on, while switches sw2, are turned off and this generates positive voltage vector V_0.
2. Switches sw3 is turned on, while switches sw1, and sw2 are turned off and this generates zero voltage vector V_1.
3. Switches sw1, and sw2 are turned on, while switches sw3, are turned off and this generates positive voltage vectorV_2.
4. Switches sw2 is turned on, while switches sw1, and sw3 are turned off and this generates zero voltage vector V_3.

The main idea of MPC is to predict the value of the control variable during next step. Prediction of circuit variables, gives the advantages of fast reference tracking. Selection of the control variables depends on the required control operation. To obtain the prediction current equation

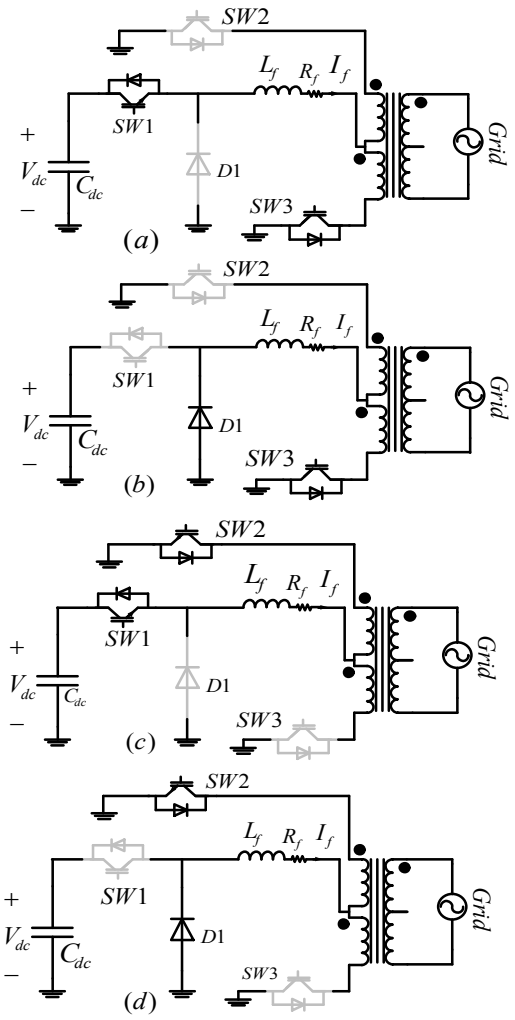

Fig. 7. Possible switching states of the three-switch inverter

of the current injected into the grid, a model for the 3S inverter is required. The model built depending on two modes of operation [21] of the inverter as follow:

Mode 1 takes place when $SW1$, and $SW3$ are on, $SW2$ and diode $D1$ are off. Applying Kirchhoff's voltage law as follow;

$$L_f \frac{di_{Lf}(t)}{dt} + i_{Lf}(t) * R_f + V_g - V_{dc} = 0 \quad (20)$$

Mode 2 takes place when $D1$, and $SW2$ are on $SW1$ and $SW3$ are off. Applying Kirchhoff's voltage law as follow;

$$L_f \frac{di_{Lf}(t)}{dt} + i_{Lf}(t) * R_f + V_g = 0 \quad (21)$$

Rearranging the equations

$$L_f \frac{di_{Lf}(t)}{dt} = V_{cf} - i_{Lf}(t) * R_f - V_g \quad (22)$$

$$L_f \frac{di_{Lf}(t)}{dt} = -i_{Lf}(t) * R_f - V_g \quad (23)$$

where v_{dc},v_g,R_f,L_f, T_s and ΔI are voltage of the dc side, grid voltage, filter inductor series resistance, filter inductor, sampling time and filter inductor current ripple.

The value of the current ripple can be controlled by the inductor value, inductor current is depicted in Fig. 7. From the graph the inductance value for the filter can be given by:

$$L = \frac{V_{dc} - V_g}{2\Delta i_L} DT_s \quad (24)$$

Typical values of Δi_L lie on the range of 10% to 20% of the full load value of the dc component I. It is undesirable to allow Δi_L to become too large; doing so would increase the peak currents of the currents if the inductor and of the semiconductor switching devices, and would increase their size and cost.

3.1. Discretization

Using the discrete form of the current equation is as follows:

$$\frac{di_{Lf}(t)}{dt} = \frac{i_{Lf}(k+1) - i_{Lf}(k)}{T_s} \quad (25)$$

The equation for predicting the load current is obtained from substituting (25) into (22) and (23), and the resulting equations are as follow:

$$I_{Lf,1}(k+1) = \frac{T_s}{L} * V_{cf} - \frac{T_s}{L} * V_g + I_{Lf}(k)\left(1 - \frac{T_s * R_f}{L_f}\right) \quad (26)$$

$$I_{Lf,0}(k+1) = I_{Lf}(k)(1 - \frac{T_s * R_f}{L_f}) - \frac{T_s}{L} * V_g \quad (27)$$

Cost function is crucial for MPC algorithm as it helps in regulating the controlled variable. Although, the current source inverter has three switches, switch SW1 is dominating in regulating the grid current. And this leads to have two cost function, cost function when switch SW1 is turned on, $G_{b,1}$, and cost function when switch SW1 is turned off, $G_{b,0}$.

$$G_{b,1} = \left|I_{Lf,1} - I_{Lf,ref}\right| \quad (28)$$

$$G_{b,0} = \left|I_{Lf,0} - I_{Lf,ref}\right| \quad (29)$$

where $I_{Lf}(k)$, $I_{Lf,1}(k+1)$, $I_{Lf,0}(k+1)$, and $I_{Lf,ref}$ are related to the inductor current, predicted inductor current when the switch is turned on, predicted inductor current when the switch is turned off, , and the reference current generated by the MPPT control, respectively.

The suggested system has five switches in total, two for the dc-dc converter and three for the dc-ac inverter, as explained. Table 3 depicts the possible switching states for the whole system. The proposed control algorithm flowchart is presented in Fig. 8. The algorithm starts with

Table 3. Switching states of the whole system.

Switching States					
Vector	Value	SW1	SW2	SW3	S1&S2
V0	V_{dc}	ON	OFF	ON	1
V1	0	OFF	OFF	ON	1
V2	$-V_{dc}$	ON	ON	OFF	1
V3	0	OFF	ON	OFF	1
V4	V_{dc}	ON	OFF	ON	0
V5	0	OFF	OFF	ON	0
V6	$-V_{dc}$	ON	ON	OFF	0
V7	0	OFF	ON	OFF	0

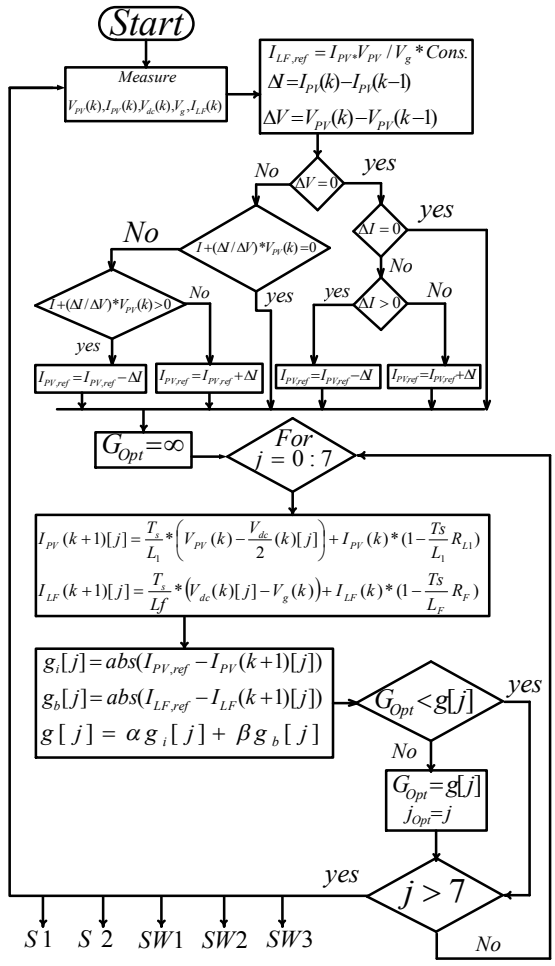

Fig. 8. Proposed MPC algorithm

measuring the required parameter for prediction and comparison such as PV's voltage and current, converter output voltage, utility voltage, and output filter current. Divergence among the present and preceding values of PV's voltage and current are calculated. After finishing this calculation, the next step is to decide to increase or decrease the PV output current by doing the following steps. If the Divergence in the voltage is zero and the difference in the current is zero, the algorithm preserve the reference current with no changes.

However, if the diversity in the voltage is equal to zero and the current diversity is more than zero, the algorithm lowers the reference current; otherwise, the algorithm raises the reference current. If the voltage diversity is not zero, the algorithm examine the $\frac{\Delta P}{\Delta V}$ term. If it is zero, the algorithm look after the reference current with no change. However, if it is greater than zero, the algorithm minifies the reference current; otherwise, the algorithm raises the reference current. For calculating the reference current for the grid side, consider that$Pin = Pout$, this simplify the selection of the reference current. Reference value of the current injected into the grid can be decided from the following equation$I_{Lf,ref} = \frac{P_{Pv}}{V_g} * const.$, where P_{Pv} is the PV available power, V_g grid voltage and $const$ is a constant is used to optimize the reference current according to the efficiency of the system. After that, prediction for the PV input current and grid current is performed for all the possible 8 states. And the cost function is optimized to select the switching state which should give the minimum error. Weighting factors α and β are used to scale the value within the cost function$g$.

4. Results

To establish and confirm the effectiveness of the proposed system, an experimental installation is arranged. Fig. 9 shows the schematic of the experimental setup. For the experimental demonstration of the proposed system, an Agilent E4360A modular solar array is used to mimic the performance of the PV module. The programmed PV module characteristics are listed in Table 4. PE Expert III with TI DSP C6713 controller is used to execute the proposed control algorithm. The 3S current source inverter is built using IXTK22N100L N-channel MOSFET. Whereas the high gain converter built using IXTK22N100L, an N-channel MOSFET, and a VS-EPU3006-N3 fast rectifier diode. The circuit inductor is made using toroid core 0077194A7. For measurement purposes, the LEM LA55-P current sensor and LEM LV25-P voltage sensor are used. The circuit parameters of the proposed system are listed in Table 5.

Table 4. PV module specification

Short Circuit Current (A)	4.2
Current at MPP (A)	3
Open Circuit Voltage (V)	25
Voltage at MPP (V)	17.8

Table 5. Circuit parameters

L1= L2	5 mH
Sampling time	10 μS
Grid Filter	3 mH
Grid Frequency	50 Hz

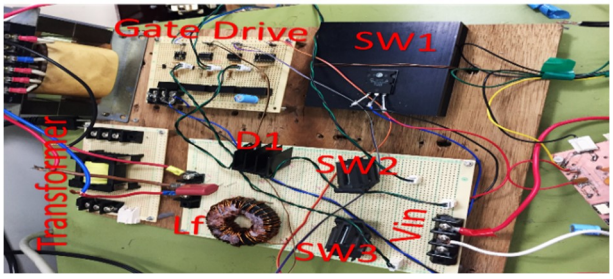

Fig. 9. Experimental setup prototype

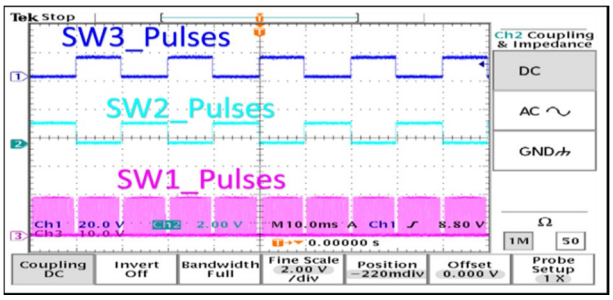

Fig. 10. Pulses of the 3S inverter

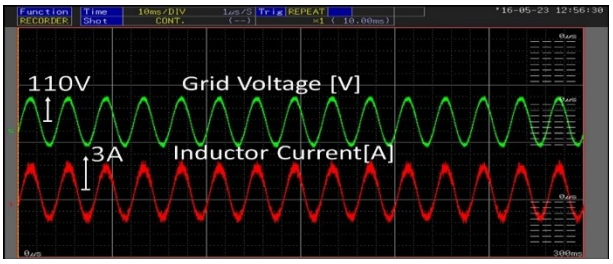

Fig. 11. Grid voltage and grid current

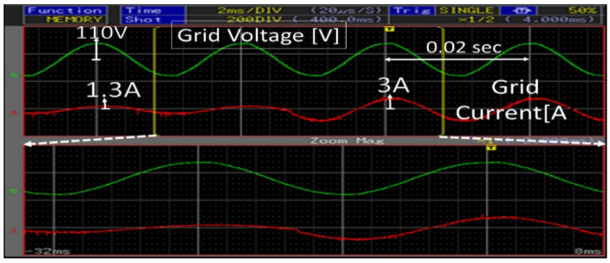

Fig. 12. Step change in grid current and grid voltage

The three switch inverter has three switches, one of them are operating at high switching frequency and the other two switches are operating at grid fundamental frequency, switches pulses are depicted in Fig. 10. For grid integrated applications, the current supplied to the grid must be sinusoidal, synchronized with the grid and has less THD. Relation between the grid voltage and injected current are depicted in Fig. 11. MPC is a robust controlled and it has distinct features, especially its transient performance. A step change is performed in the grid current and is depicted in Fig. 12. Switch SW1 is the only switch of the inverter

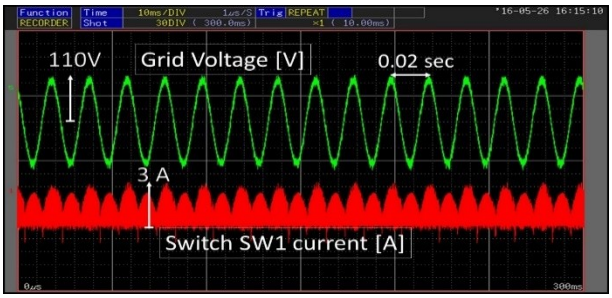

Fig. 13. Grid voltage and switch SW1 current.

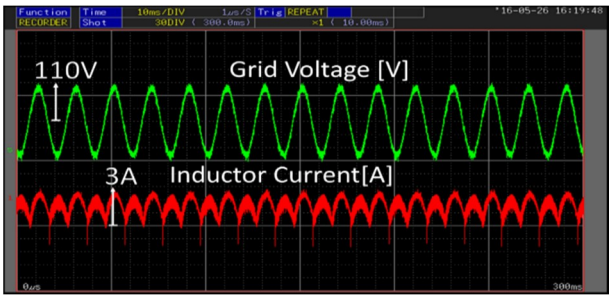

Fig. 14. Grid voltage and filter inductor current.

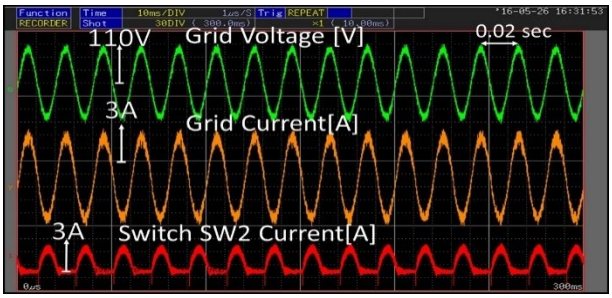

Fig. 15. Grid voltage, grid current and switch SW2 current.

switches that operates at high switches frequency, and as it is modulation in rectified sinusoidal wave form, it is current is switched and has the shape of rectified sinusoidal waveform. Fig. 13 is a depiction of the grid voltage and switch SW1 current. The value of the filter inductance controls the amount of grid current ripple. The filter has a rectified current synchronized with the grid voltage, due to the modulation style. Fig. 14 depicts the grid voltage and filter current. Switch SW2 is operating at fundamental frequency and it remains on during the whole positive half cycle of the grid voltage, and becomes off in the negative half cycle. Relation between, grid voltage, grid current and switch SW2 current is depicted in Fig. 15. Switch SW3 is operating in the counter part with switch SW2. SW also is operating at the fundamental frequency and it is on the whole time during the negative half cycle of the grid.

MPC is a committed control technique owing to its perfect transient response and ability of include system nonlinearity. Simulation comparison between the well-known proportional–integral (PI) control and MPC in controlling the current injected into the grid is shown in

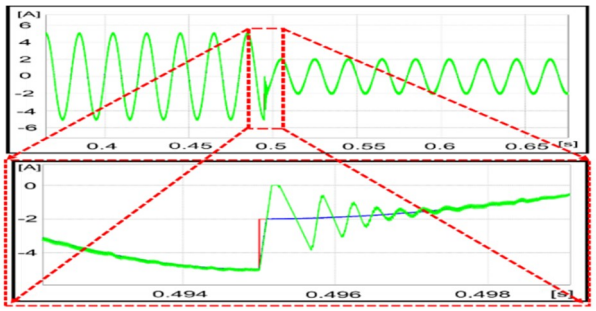

Fig. 16. Comparison between PI and MPC

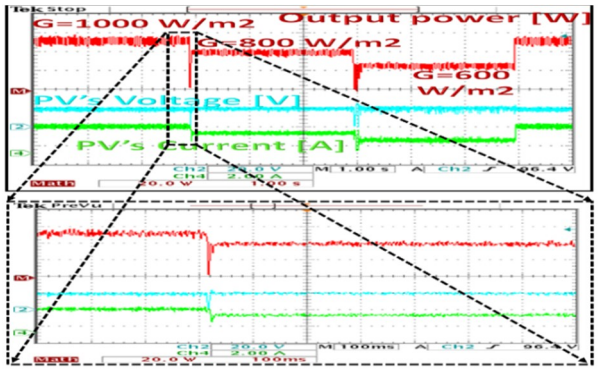

Fig. 17. MPPT-MPC algorithms results with radiation change from 1000 to 800 to 600 and back to 1000 W/m2.

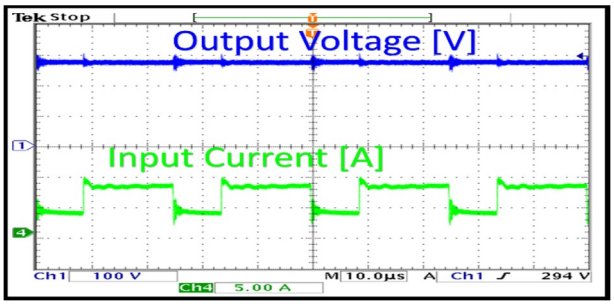

Fig. 18. Output voltage and input current

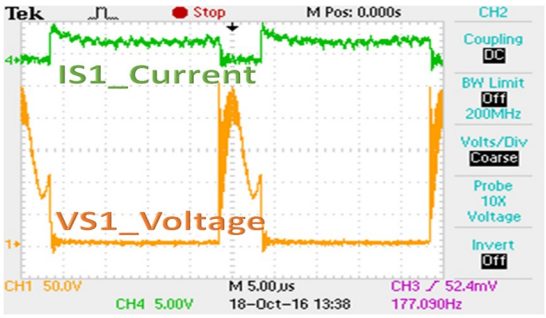

Fig. 19. Switch voltage and switch current.

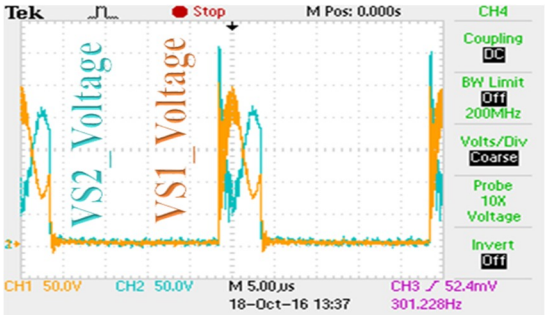

Fig. 20. Switch SW1 voltage and switch SW2 voltage.

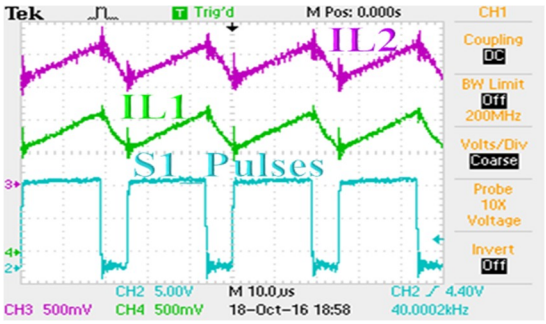

Fig. 21. Inductor L1 current, inductor L2 current and switch pulse

Fig. 16. The reference current changes from 5 to 2 A. The figure shows that the MPC succeeds in tracking the reference current without any overshoot, and the settling time is very small. Meanwhile, the PI controller suffers from overshoot, and the settling time is longer than the MPC settling time.

Solar radiation is a main factor in determining the maximum available power from the PV module. A study case is depicted in Fig. 17. In this case radiation changed from 1000, to 800, to 600 W/m^2. Overshoot is observed and maximum power is achieved. At G=600 W/m^2, output power from the PV is 24 W, and at G=800 W/m^2 is 40 Wand the power at G=1000 W/m^2 is 48W. The algorithm is faster in case of power up than when the radiation is decreased. At G=800 W/m^2 is 40 Wand the power at G=1000 W/m^2 is 48W. No overshoot is observed. And transient time is very small. The MPPT-MPC algorithm succeeded in tracking the maximum power with very small transient time. Fig. 18 depicts output voltage and input current, in this figure output voltage is 273 V which means the voltage gain at this point is 9 times the input voltage. Also input current change from 8 Amp when the switch is turned on to 4 Amp when the switch is turned off. Fig. 19 represents the voltage and current of switch S1 while Fig. 20 represents the voltages of switches S1 and S2. The two inductors L1 and L2 are symmetrical. According to the circuit configuration the two inductors are charging in parallel when the switches are turned on and discharged in series configuration when the switches are triggered to be off, Fig. 21 depicts the currents of IL1 and IL2 and switch pulses. Diodes D1 and D3 have forward bias when the switches S1 and S2 are turned on while D3 becomes on when the switches are turned off. Fig. 22 combine the diodes reverse voltage and switch S1 reverse voltage. Fig.

Table 6 Performance comparison among the proposed and other high step-up converters

	[25]	[25][26]	[27]	[28]	[29]	[30]	Flyback	Proposed
Voltage gain	$\frac{(1+n)}{(1-D)}$	$\frac{(1+n+nD)}{(1-D)}$	$\frac{(1+n)}{(1-D)}$	$\frac{(1+nD)}{(1-D)^2}$	$\frac{1}{(1-D)^2}$	$\frac{(1+D)}{(1-D)}$	$\frac{nD}{(1-D)}$	$\frac{(3+D)}{(1-D)}$
Number of MOSFETs	1	1	1	1	1	1	1	2
Number of power diodes	3	5	3	4	3	4	1	3
Number of capacitors	3	5	4	3	2	1	1	3
Number of transformers	1	1	1	1	0	0	1	0
Number of inductors	0	0	1	1	2	2	0	2
Voltage stress of active switch	$\frac{V_o}{(1+n)}$	$\frac{V_o}{(1+n+nD)}$	$\frac{V_o}{(1+n)}$	$\frac{V_o}{(1+nD)}$	V_o	V_o	$\frac{V_o}{(n)}+V_{in}$	$\frac{V_o+V_{in}}{4}$
Maximum voltage stress among all power diodes	V_o	$\frac{nV_o}{(1+n+nD)}$	$\frac{nV_o}{(1+n)}$	$\frac{nV_o}{(1+nD)}$	V_o-V_{in}	V_o-V_{in}	V_o+nV_{in}	$\frac{V_o+V_{in}}{2}$

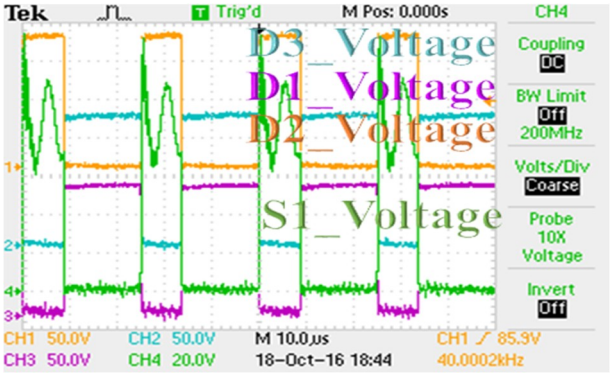

Fig. 22. Switch S1 voltage and Diodes D1, D2 and D3 voltages

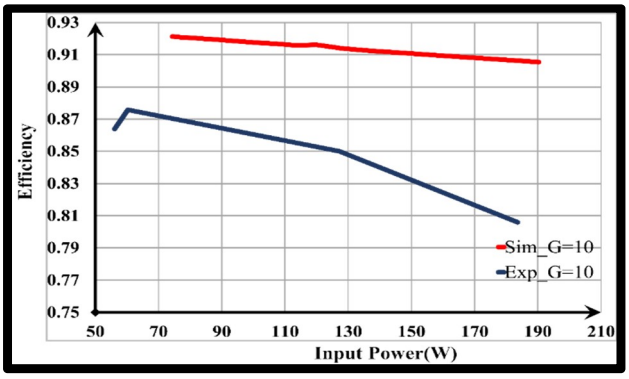

Fig. 23. Experimental and simulated efficiency vs input power with voltage gain M=10

23 depict the relation between the converter efficiency and input power. Red line is the simulated results and based on the parameters depicted in Table 2, while the dark line is the experimental results. Voltage gain of the converter is set to 10 times and input power range up to 200 W. simulated efficiency is around 91 % while experimental one is around 85 %. Table 6 is a performance comparison among the proposed converters and other high step-up converters. Topologies proposed in [15, 21-23] and the flyback converter have promising voltage-gains, but the existence of high-frequency transformer affects the overall efficiency of the converter. The converter efficiency decreases as the number of turns increases. Topologies presented in [24] and [25] have promising voltage-gain also, but the overall efficiency are not so high due to the high voltage stresses on the power switch. Although the proposed high gain dc-dc converter has two switches and three diodes, it has the highest efficiency amongst other topologies. The high efficiency occurred due to the reduced voltage stresses on the power MOSFETs and diodes. The second advantages of the proposed converter that is can provides high voltage gain without the need for a high frequency transformer.

5. Conclusions

This paper offered two-stage inverter for reduced power grid-tied PV applications. In the first-stage high-gain and high-efficiency dc-dc converter based on the Cockcroft-Walton multiplier were proposed. The proposed DC-DC converter was able to deliver high-voltage ration with very-high efficiency. With voltage ratio around 19 time, the proposed converter efficiency was found around 94%. The Second-stage was utilizing the 3S current-source inverter. The 3S inverter has three power devices and one transformer. One of the 3S inverter's switches was operating at high-switching frequency and the other two switches were operating at fundamental grid frequency. The 3S had the advantages of galvanic isolation, less conduction and switching losses. A powerful and accurate finite-set model predictive control were proposed and developed to extract the maximum power from the PV module, and inject a sinusoidal wave current into the grid. Experimental results for the whole system were portrayed through the paper. The experimental results of the high-gain converter was consistent with the calculated values and it showed an experimental efficiency around 90 % at

voltage-gain around 10 times and input power was 100W. MPPT and grid current control both were controlled via the MPC algorithm. The investigated MPC algorithms showed a very fast transient responses and powerful ability to control the grid current

Acknowledgements

The author would like to thank the Egyptian higher ministry of education for supporting him to complete his study in Japan. This work was supported by JSPS KAKENHI grant number 15K05929.

References

[1] B. Sahan, S. Member, A. N. Vergara, N. Henze, A. Engler, and P. Zacharias, "A Single-Stage PV Module Integrated Converter Based on a Low-Power Current-Source Inverter," *IEEE Trans. Ind. Electron.*, vol. 55, no. 7, pp. 2602-2609, 2008.

[2] K. Tattiwong and C. Bunlak "Novel clamp-mode coupled-inductor boost converter with high step-up voltage gain," *J Electr Eng Technol.2017*; 12(2): 809-819

[3] O. Abdel-Rahim and H. Furiato, "Switched inductor quadratic boosting ratio inverter with proportional resonant controller for grid-tie PV applications," *in IECON 2014 - 40th Annual Conference of the IEEE Industrial Electronics Society*, 2014, pp. 5606-5611.

[4] O. Abdel-Rahim, M. Orabi, and M. E. Ahmed, "Development of high-gain high-efficiency grid-connected inverter for PV Module," *in Power Electronics for Distributed Generation Systems (PEDG)*, 2010 2nd IEEE International Symposium on, 2010, pp. 368-373.

[5] M. E.-S. Ahmed, M. Orabi, and O. M. AbdelRahim, "Two-stage micro-grid inverter with high-voltage gain for photovoltaic applications," *IET Power Electron.,* no. November 2012, pp. 1-10, Aug. 2013.

[6] D. Navamani, R. Jegatheesan and A. Lavanya "High step-up dc-dc converter by switched inductor and voltage multiplier cell for automotive applications," *J Electr Eng Technol.2017*, vol. 12, no. 1, pp. 189-197, 2017.

[7] D. H. Kim, H. W. Kim, J. H. Park, and H. J. Jeon, "High efficiency high-step-up single-ended DC/DC converter with small output voltage ripple," *J. Power Electron.*, vol. 15, no. 6, pp. 1468-1479, 2015.

[8] D. Dc, L. Configurations, Q. Li, P. Wolfs, and S. Member, "A Review of the Single Phase Photovoltaic Module Integrated Converter Topologies With Three," *IEEE Trans. POWER Electron.*, vol. 23, no. 3, pp. 1320-1333, 2008.

[9] O. Abdel-Rahim, H. Funato, and J. Haruna, "Z-source with voltage multiplication inverter for grid-tie photovoltaic applications," in 2015 *IEEE International Telecommunications Energy Conference* (*INTELEC*), pp. 1-6, 2015.

[10] T. K. S. Freddy, N. A. Rahim, Wooi-Ping Hew, and Hang Seng Che, "Comparison and Analysis of Single-Phase Transformerless Grid-Connected PV Inverters," *IEEE Trans. Power Electron.*, vol. 29, no. 10, pp. 5358-5369, Oct. 2014.

[11] D. Thena, A. Ahmed, B. Choi, J. Park, and H. Park "Independent MPP tracking method of hybrid solar-wind power conditioning systems using integrated dual-input single-pwm-cell converter topology," *J Electr Eng Technol.2017*, vol. 12, no. 2, pp. 790-802, 2017.

[12] D. Meneses, F. Blaabjerg, Ó. García, and J. A. Cobos, "Review and comparison of step-up transformerless topologies for photovoltaic AC-module application," *IEEE Transactions on Power Electronics*, vol. 28, no. 6. pp. 2649-2663, 2013.

[13] O. Abdel-Rahim, M. Orabi, and M. E. Ahmed, "Buck-boost interleaved inverter for grid connected Photovoltaic system," *in 2010 IEEE International Conference on Power and Energy*, 2010, pp. 63-68.

[14] O. Abdel-Rahim, H. Funato, and H. Junnosuke, "Grid-tie switched inductor with voltage multiplier inverter," *in 2014 IEEE Energy Conversion Congress and* Exposition (*ECCE*), 2014, pp. 2221-2226.

[15] H. Xiao, S. Xie, Y. Chen, and R. Huang, "An Optimized Transformerless Photovoltaic Grid-Connected Inverter," *IEEE Trans. Ind. Electron.*, vol. 58, no. 5, pp. 1887-1895, May 2011.

[16] B. Yang, W. Li, Y. Gu, W. Cui, and X. He, "Improved Transformerless Inverter With Common-Mode Leakage Current Elimination for a Photovoltaic Grid-Connected Power System," *IEEE Trans. Power Electron.*, vol. 27, no. 2, pp. 752-762, Feb. 2012.

[17] B. Gu, J. Dominic, J. Lai, C.-L. Chen, T. LaBella, and B. Chen, "High Reliability and Efficiency Single-Phase Transformerless Inverter for Grid-Connected Photovoltaic Systems," *IEEE Trans. Power Electron.*, vol. 28, no. 5, pp. 2235-2245, May 2013.

[18] O. Abdel-Rahim, H. Funato, and J. Haruna, "Pseudo single stage flyback current source inverter for grid connected PV applications," *in IECON 2015 - 41st Annual Conference of the IEEE Industrial Electronics Society*, 2015, pp. 1-6.

[19] T. Kerekes, R. Teodorescu, P. Rodriguez, G. Vazquez, and E. Aldabas, "A New High-Efficiency Single-Phase Transformerless PV Inverter Topology," *IEEE Trans. Ind. Electron.*, vol. 58, no. 1, pp. 184-191, Jan. 2011.

[20] J. Rodríguez, S. Member, J. Pontt, C. A. Silva, P. Correa, P. Lezana, P. Cortés, S. Member, and U. Ammann, "Predictive Current Control of a Voltage Source Inverter," vol. 54, no. 1, pp. 495-503, 2007.

[21] P. Cortes, A. Wilson, S. Kouro, J. Rodriguez, and H. Abu-Rub, "Model predictive control of multilevel cascaded H-bridge inverters," *IEEE Trans. Ind. Electron.*, vol. 57, no. 8, pp. 2691-2699, 2010.
[22] O. Abdel-Rahim, H. Funato, and J. Haruna, "Novel Predictive Maximum Power Point Tracking Techniques for Photovoltaic Applications," *J. Power Electron.*, vol. 16, no. 1, pp. 277-286, Jan. 2016.
[23] B. Axelrod, Y. Berkovich, and A. Ioinovici, "Structures for Getting Transformerless Hybrid DC - DC PWM Converters," *IEEE Trans. CIRCUITS Syst.*, vol. 55, no. 2, pp. 687-696, 2008.
[24] L. Yang, T. Liang, and J. Chen, "Transformerless DC-DC Converters With High Step-Up Voltage Gain," *IEEE Trans. Ind. Electron.*, vol. 56, no. 8, pp. 3144-3152, Aug. 2009.
[25] S. M. Chen, T. J. Liang, L. S. Yang, and J. F. Chen, "A safety enhanced, high step-up DC-DC converter for AC photovoltaic module application," *IEEE Trans. Power Electron.*, vol. 27, no. 4, pp. 1809-1817, 2012.
[26] S. Changchien, T. Liang, J. Chen, and L. Yang, "Novel High Step-Up DC-DC Converter for Fuel Cell Energy Conversion System," *IEEE Trans. Ind. Electron.*, vol. 57, no. 6, pp. 2007-2017, Jun. 2010.
[27] K. B. Park, G. W. Moon, and M. J. Youn, "High step-up boost converter integrated with a transformer-assisted auxiliary circuit employing quasi-resonant operation," *IEEE Trans. Power Electron.*, vol. 27, no. 4, pp. 1974-1984, 2012.
[28] C.-L. Shen and P.-C. Chiu, "Buck-boost-flyback integrated converter with single switch to achieve high voltage gain for PV or fuel-cell applications," *IET Power Electron.*, vol. 9, no. 6, pp. 1228-1237, 2016.
[29] O. López-Santos, H. Valderrama-Blavi, G. García, D. O. Mercuri, and L. Martínez-Salamero, "Efficiency analysis of a sliding-mode controlled quadratic boost converter," *IET Power Electron.*, vol. 6, no. 2, pp. 364-373, Feb. 2013.
[30] O. Abdel-Rahim, M. Orabi, E. Abdelkarim, M. Ahmed, and M. Z. Youssef, "Switched inductor boost converter for PV applications," *in 2012 Twenty-Seventh Annual IEEE Applied Power Electronics Conference and Exposition* (*APEC*), 2012, pp. 2100-2106.

Omar Abdel-Rahim received his B.S. and M.S. degrees in Electrical Engineering, from the Faculty of Engineering, Aswan University, Aswan, Egypt, in 2009 and 2012, respectively. He is presently working towards his Ph.D. in the Department Of Electrical Engineering, Utsunomiya University, Utsunomiya, Japan. From 2009-2012, he was a Research Assistant with the Aswan Power Electronic Application Research Center (APEARC) Aswan, Egypt. Since 2010, he has been an Assistant Lecturer in the Department of Electrical Engineering, Aswan University. In 2012, he joined the Texas A&M University at Qatar as a Research Associate. He has authored or coauthored over 20 papers in leading international conferences and journals, mainly on the topics of grid connected inverters and multiphase matrix converters. His current research interests include multiphase machines drives, predictive control, renewable energy, smartgrids, and DC-AC converters.

Hirohito Funato was born on February 26, 1964, in Fukushima, Japan. He received his B.S., M.S., and Ph.D. degrees in Electrical Engineering from Yokohama National University, Yokohama, Japan, in 1987, 1989, and 1995, respectively. He worked at the Tokyo Electric Power Company from 1989 to 1991. He joined the Faculty of Engineering, Utsunomiya University, Utsunomiya, Japan, in 1995, where he is presently working as a Professor. His current research interests include applications of power electronics to power systems, digital control of power electronic circuits, renewable energy, etc. He received a PCC2007 Best Paper Award in 2007, and IEEJ Paper Presentation Awards in 1994 and 1997. Dr. Funato is a member of the IEEJ, IEEE PELS, IAS and IES.

Junnosuke Haruna was born in Hokkaido, Japan, in 1983. He received his B.S., M.S., and Ph.D. degrees in Electrical Engineering from Nagaoka University of Technology, Nagaoka, Japan, in 2006, 2008, and 2011, respectively. He joined the Department of Electrical Engineering, Faculty of Science and Technology, Tokyo University of Science, Noda, Japan, as an Assistant Professor, in 2011. He has been with Utsunomiya University, Utsunomiya, Japan, as an Assistant Professor, since 2014. His current research interests include power electronics, motor control, and electric vehicles. He is a Member of the Institute of Electrical Engineers of Japan, and a Member of IEEE.